A comparison of de-alloying crystalline and amorphous multicomponent Au alloys

Elsevier Editorial System(tm) for Intermetallics
Manuscript Draft

Manuscript Number: INTERMETALLICS-D-15-00237R1

Title: A Comparison of De-alloying Crystalline and Amorphous Multicomponent Au Alloys

Article Type: Research Paper

Section/Category: Metallic glasses

Keywords: A) porous materials, A) metal glasses; B) corrosion, B) diffusion; D) interfaces

Corresponding Author: Dr. Federico Scaglione, Ph.D

Corresponding Author's Institution: Università di Torino

First Author: Federico Scaglione, Ph.D.

Order of Authors: Federico Scaglione, Ph.D.; Federica Celegato, Dr.; Paola Rizzi, Professor; Livio Battezzati, Professor

Abstract: The formation of nanoporous metals by de-alloying is not fully disclosed especially in the case of complex alloys such as amorphous ones. Here a crystalline porous scaffold made of ligaments and pores must originate from a matrix of diverse structure.
In this paper a contribution to the field is achieved by pointing out differences that have been noticed comparing ligaments in de-alloyed materials obtained from either amorphous or crystalline precursors. Two multicomponent Au-based alloys in the form of ribbons, an amorphous Au40Cu28Ag7Pd5Si20 and a polycrystalline Au31Cu41Zn12.8Mn15.2, have been chemically de-alloyed in same conditions. The resulting nanoporous materials have been characterized by microscopy and diffraction and the kinetics of the process have been determined. The morphology of ligaments is definitely diverse as well as the size of crystals. This is proven by the ratio, r, between the ligament size and the size of scattering domains obtained by Rietveld analysis: the ligaments formed from the amorphous precursor are constituted by several crystals (r⁄5) whereas ligaments from crystalline alloys contain a single domain (r⁄1). The results are discussed in terms of surface diffusion and mechanism of growth of ligaments.

A Comparison of De-alloying Crystalline and Amorphous Multicomponent Au Alloys

F. Scaglione[a], F. Celegato[b], P. Rizzi[a], L. Battezzati[a]
[a]Dipartimento di Chimica and NIS, Università di Torino, V. Giuria 7, 10125 Torino, Italy.
[b]INRIM, Strada delle Cacce 91, 10135 Torino, Italy

Corresponding author: federico.scaglione@unito.it

Abstract

The formation of nanoporous metals by de-alloying is not fully disclosed especially in the case of complex alloys such as amorphous ones. Here a crystalline porous scaffold made of ligaments and pores must originate from a matrix of diverse structure.

In this paper a contribution to the field is achieved by pointing out differences that have been noticed comparing ligaments in de-alloyed materials obtained from either amorphous or crystalline precursors. Two multicomponent Au-based alloys in the form of ribbons, an amorphous $Au_{40}Cu_{28}Ag_7Pd_5Si_{20}$ and a polycrystalline $Au_{31}Cu_{41}Zn_{12.8}Mn_{15.2}$, have been chemically de-alloyed in same conditions. The resulting nanoporous materials have been characterized by microscopy and diffraction and the kinetics of the process have been determined. The morphology of ligaments is definitely diverse as well as the size of crystals. This is proven by the ratio, *r*, between the ligament size and the size of scattering domains obtained by Rietveld analysis: the ligaments formed from the amorphous precursor are constituted by several crystals (r~5) whereas ligaments from crystalline alloys contain a single domain (r~1). The results are discussed in terms of surface diffusion and mechanism of growth of ligaments.

Keywords: A) porous materials, A) metal glasses, B) corrosion, B) diffusion, D) interfaces.

1. Introduction

De-alloying is the corrosion process, either chemical or electrochemical, in which less noble metal are selectively removed from an alloy, leading to a material made of interconnecting ligaments and pores [1]. The resulting meso/nanoporous structure is proposed for application in various field such as catalysis [2], sensors, hydrogen storage, molecular sieves, surface-enhanced Raman scattering [3] and actuators [4]. One requirement for application is a tunable ligament size made of an almost pure inert metal [5], although small amounts of impurity elements could be crucial for improving the sensing or chemical activity [2].

The de-alloying has been studied in a number of binary alloys, usually solid solutions of Au with Cu [6] and Ag [7, 8]. The main aspects of the mechanisms and the parameters for de-alloying of crystalline alloys have been identified by the studies of Erlebacher [9, 10], Pickering [11, 12] and Sieradzky [13]: the model that has been proposed takes into account surface diffusion, capillary forces and kinetics of electrochemical dissolution. On selective removal of less noble elements, the noble ones reorganize in islands by surface diffusion of adatoms on the underlying crystals forming hillocks which are then subject to undercutting, spreading ligaments and porosities into the bulk [1]. Therefore, the nanoporous material has the same crystal structure as the matrix, i. e. *fcc*, and the original grain microstructure is retained [14]. If the precursor structure has complex crystal lattice or is amorphous, the nanoporous material has again *fcc* structure, but ligaments are made of multiple crystals [15, 16, 17]. The mechanism of formation of ligaments is not yet fully disclosed and this study is aimed at elucidating some aspects of it by comparing the nanoporous gold (NPG) obtained by chemical de-alloying two Au-based multicomponent precursors: a $Au_{40}Cu_{28}Ag_7Pd_5Si_{20}$ [18] amorphous alloy whose complex composition reflects the requirement for having good glass forming ability, and a polycrystalline $Au_{31}Cu_{41}Zn_{12.8}Mn_{15.2}$ [19]. Both of them have been synthesized by rapid solidification ensuring the achievement of a single homogeneous phase.

2. Experimental

Ingots of $Au_{31}Cu_{41}Zn_{12.8}Mn_{15.2}$ and $Au_{40}Cu_{28}Ag_7Pd_5Si_{20}$ [20] were prepared by arc-melting the mixture of commercially pure elements in Ti gettered Ar atmosphere. Ribbons 25 μm thick and 2 mm wide were obtained by melt-spinning the master alloy with a linear velocity of the copper wheel of 22 m/s. The former alloy solidifies as an *fcc* solid solution, the latter as a glass.

Ribbons of the two alloys have been free corroded in 14.4 M, 10 M and 5 M HNO_3 aqueous solution for etching time of 1 month at 255 K, 24 h at 293K and 6 h at 343 K and 363 K aiming at complete de-alloying through the thickness. They have been analysed before and after etching using X-ray diffraction (XRD) in Bragg-Brentano geometry with monochromatic Cu Kα radiation, Scanning Electron Microscopy (SEM), Energy Dispersive X-ray Spectroscopy (EDS) (calibrated with a Co standard), Transmission Electron Microscopy (TEM) after mechanical thinning.

All electrolytes have been prepared from chemical grade reagents and deionized water. Characterization of the porous structure has been performed by measuring the average ligament size using a software for image analysis and checked also with some manual tests employing the intercept method.

3. Results

3.1 Characterization and free corrosion of a multicomponent crystalline alloy

$Au_{31}Cu_{41}Zn_{12.8}Mn_{15.2}$ is a 14 carats alloy, whose composition was designed to be free of allergenic Ni, a major whitener of most commercial white golds [11]. In addition to being well characterized in the Authors' laboratory, this alloy has been selected because it is multicomponent and the amount of the most noble element, i.e. Au, is less than the parting

limit for de-alloying of Au based alloys [5, 21]. The melt spun ribbon is constituted by columnar grains of a *fcc* solid solution which grew from the surface in contact with the wheel of the melt spinning apparatus in the direction along which heat was subtracted during the rapid quenching process. High resolution SEM images of the top view of as-spun ribbons de-alloyed in 14.4 M at different temperatures are shown in Fig. 1a to 1d. The porous structure is similar also inside the cross section and uniform for every sample. The size of ligaments increases as a function of temperature and electrolyte concentration (see Figs. S1 and S2 in supporting information). The samples are fully de-alloyed as shown by the image of the cross section (Fig. 1e); it is apparent that the ribbon underwent intergranular fracture and, therefore, the elongated grains produced by the solidification are recognized. The average size resulting from at least one hundred ligaments, is reported for all samples in Fig. 1f. The scatter associated to each measurement is the standard deviation with respect to the average size. Ligaments and pores coarsen on increasing the processing temperature. No significant differences have been observed in ligament size between air and wheel-side of the melt spun ribbon. EDS analyses show the ligaments are made of almost pure Au for samples de-alloyed in 14.4 M, 10 M, and 5 M HNO_3 at the highest temperatures whereas after de-alloying at the lowest temperature Cu, Mn and Zn have still been detected in the amount of ~18, 7 and 4 at. %, respectively.

The close-up image of ligaments and pores in Fig. 2a shows the interconnected network within a single crystal of NPG. Surfaces display varied curvature with smooth transition from place to place and pores are rounded in several locations.

Diffraction patterns of the samples de-alloyed in 14.4 M HNO_3 at different temperatures indicate that the *fcc* solid solution in the as spun ribbon is completely de-alloyed except at 255 K (Fig. 3): in the former case only *fcc* reflections of almost pure gold appear, in the latter low intensity reflections of the starting *fcc* solid solution are still recognized. The lattice parameter, a_0, is close to the value of pure Au (a_0 = 4.08 Å) within the experimental error for all samples, except that prepared at 255 K and 5 M at low temperatures in which residual percentage of other elements inside ligaments is retained. A texture effect on (111) and (200) reflections is observed in patterns taken on the air side (Fig. 3, inset) confirming the crystal orientation is maintained in the porous gold after de-alloying. The same behaviour has been noticed for samples de-alloyed in 10 M and 5 M HNO_3 (Supporting information, Figs. S3 and S4). The size of scattering domains has been evaluated according to the Rietveld method [22] and results of the same order as that of ligaments (data are collected in Table 1, supporting information).

3.2 Characterization and free corrosion of a multicomponent $Au_{40}Cu_{28}Ag_7Pd_5Si_{20}$ amorphous alloy

The $Au_{40}Cu_{28}Ag_7Pd_5Si_{20}$ composition has been developed to improve the glass forming ability of Au-based glassy alloys [23]. Glass formation in these alloys is favoured by the negative enthalpy of mixing between the main components in the liquid state which implies the occurrence of short range order. In glass-forming melts based on Au a preferential interaction occurs between the metalloid, Si, and the metal atoms, therefore the Si is mostly surrounded by metals in the glass structure, as typical for metal-metalloid systems [24]. Among the component elements, the Si is less noble and, therefore, its removal initiates the etching process by providing sites for dissolution of the surrounding less noble metals which lead to electrolyte percolation for continuing the process in the interior of the ribbon. The glass structure is then disrupted and the local composition is shifted outside the glass forming range. The remaining noble atoms are then left free to group by moving to short distances. A large number of crystals of nanometre size having compact structure is formed as shown by TEM images of samples de-alloyed for 30 s in 1 M HNO_3 [17] (Figs. S5, Supporting information). After 5 minutes the crystals appear to coalesce into ligaments and with pores in between (Figs. S6, Supporting information). These images were collected with samples mechanically thinned before de-alloying, a measure taken to avoid any artifact in the preparation of transparent samples. For longer de-alloying times significant information is

provided by the SEM images (Fig. 2b) which show that ligaments have grown in multiple locations to the size of hundreds of nanometre while being made of several crystals. It is apparent that surface diffusion of the adatoms along the surface/electrolyte interface has extensively occurred causing growth of the impinged crystals forming ligaments. The reduction of surface energy has also driven the coalescence of pore. The kinetics of the diffusional mechanism of de-alloying was earlier reported both in the case of potentiostatic etching in 1 M HNO_3, H_2SO_4 and $HClO_4$ [17] and of free corrosion [20]. Since amorphous alloys are corrosion resistant, complete de-alloying of the ribbon can be achieved in reasonable times only at temperatures from 70 °C and above. Results on the size of ligaments as a function of temperature are reported in Fig. 1f and collected in Tab. 2 of supplementary information. The size is comparable to that of ligaments obtained from the crystalline alloy at all temperatures. XRD patterns display broad reflections of the *fcc* phase indicating the occurrence of fine scattering domains (Fig. 4). Their size was obtained from Rietveld analysis and is given in Tab. 2 as well.

EDS performed on areas of the surface reveals the predominance of Au but also substantial quantities of the other elements. Since the crystallization of Au implies that Si has been removed from the uppermost layer, the measured overall Si content must originate from the underlying glassy phase. This is 6 at % after 15 minutes de-alloying, detected at spots after 30 minutes, and below the detection limit from 1 h onwards. The amount found for metal elements is due to contribution of both the de-alloyed layer and of the amorphous substrate. After 15 and 30 minutes the metal concentrations are, respectively: 19 and 7 at % for Cu, 3 and 2 at % for Ag, 1 at % and below limit for Pd. These average values result from several measurement on different parts of the surface and are affected by a scatter of the order of 30%. However, they exceed those expected if the elements were contained only in the amorphous part. For longer times, inspection of spectra revealed clearly traces of Cu, Ag and Pd in various locations although their overall amount cannot be quantified with precision [17]. It is, therefore, concluded that these elements remain trapped to some extent in the protrusions and ligaments.

A close up view of ligaments and pores is shown in Fig. 2b. The main feature to be noted is that the ligaments are made of several crystals whose boundaries are visible on the external surface. The size of these grains is of the same order as that of scattering domains. This microstructure indicates that each crystal grew separately until impingement with one another. The shape of ligaments is less homogeneous than in Fig. 2a, containing some crystal agglomerates and thinner bridged in between.

4. Discussion

4.1 De-alloying of Crystalline vs Amorphous Alloys

The formation and evolution of ligaments and pores in homogeneous crystalline solid solutions i.e. Au-Ag or Au-Cu, is understood according to the model put forward by Erlebacher and co-workers [7] which accounts for surface diffusion of atoms and capillary forces competing during the de-alloying process. The less noble metal is dissolved layer by layer letting gold free to move by surface diffusion to form islands and then hills. As more atoms are removed, the mounds are undercut and a skeleton of ligaments of Au is formed in the bulk of the original grains of the alloy. Coarsening of ligaments due to a capillary-driven mechanism, or de-roughening, occurs with time at length scales of the order of the diffusion distance. The de-alloying of the multicomponent alloy employed in this work appears to follow closely this mechanism in all instances. It is apparent that Au atoms diffuse on the surface of the *fcc* phase and cluster to get a complete shell of nearest neighbours. Therefore, the original grains to which the ligaments are bonded are progressively filled with pores.

The local order in metal-metalloid amorphous alloys is represented by polyhedra which contain at their centre the metalloid atom, e. g. capped trigonal prisms of metal atoms having varied local distortion. The prototype $Au_{86}Si_{16}$ from which the glassy alloy employed in this study was derived, was shown to conform to this picture [24]. Usually the density of

amorphous alloys is slightly less than that of the corresponding crystals (of the order of a few units percent [25]). The metal atoms then have slightly looser bonding and coordination in the glassy structure with respect to the crystalline counterpart. The combination of metal atoms contained in $Au_{40}Cu_{28}Ag_7Pd_5Si_{20}$ increases the glass forming tendency by reducing the chance of nucleating crystals on quenching. It is reckoned the metal atoms mix randomly in the coordination shell of Si of which the Au constitutes about one half. These Au first neighbours are liberated by dissolution of less noble elements and move as adatoms creating sites for aggregation of further noble atoms into their stable *fcc* structure. This occurs at random in a large number of places so that numerous domains grow as a function of time until they impinge on each other forming ligaments. The size of the crystalline domains should then be of the order of the diffusion distance in the given condition of temperature and electrolyte concentration. The morphology of ligaments (Fig. 2) obtained from crystalline alloys are smooth and roundish while ligaments originated from amorphous precursors are knobby and rough suggesting a difference in mechanism of de-alloying between crystalline and amorphous precursors. This is then demonstrated by considering the ratio, *r*, between the dimension of scattering domains from Rietveld analyses of the pertinent XRD patterns and the ligament size as measured by high resolution SEM images (Fig. 5) which is close to one for the crystalline alloy and between 4 and 5.5 for the amorphous alloy indicating that each ligament is composed of multiple crystals. The decreasing trend of *r* as a function of temperature is indicative of the expected coarsening of crystal domains.

A common feature of both crystalline [26] and amorphous alloys is that their de-alloyed products retain amounts of less noble metal atoms which are apparently trapped in the crystals by the movement of the Au atoms. The combination of morphology and residual elements occurring only in the case of de-alloying a metallic glass might be of relevance for specific applications in catalysis or sensing [6, 27].

4.2 Surface Au diffusivity in free corrosion condition

Diffusion of adatoms along the surface/electrolyte interface in de-alloying is driven by the decrease of interfacial energy due to the reduction of surface area analogously to coalescence of particles in de-roughening of Au electrodes [28, 29]. The rate of increase in radius of the coarsening particles, r(t), is given by $\frac{d(r^4)}{dt} = \frac{2\gamma a_0^4 D_s}{kT}$. The surface diffusivity, D_s is obtained by integrating this equation and by using the following parameters [30, 31, 32]: k the Boltzmann constant, T the dealloying temperature, γ the surface energy (of the order of 1 Jm^{-2} for Au in contact with an aqueous solution [28]), t the dealloying time, a_0 a jump distance assumed to be of the order of the lattice constant of Au (4.08×10^{-10} m), *r* is the ligament size when the precursor is a crystalline alloy or the dimension of scattering domains in the case of an amorphous one [20]. D_s values obtained for the crystalline alloy increase as a function of temperature with an Arrhenius dependence and with electrolyte concentration (Fig. 6, and values collected in Tab. 3, supporting information). They fall in the range of the diffusivity values reported in the literature for electrode de-roughening at comparable temperatures [25, 33, 34]. The activation energy for surface diffusion, E_a, has been obtained as 78 ± 4, 93 ± 7 and 97 ± 5 kJ mol^{-1} respectively in 14.4, 10 and 5 M HNO_3. (Table 4, supporting information). Values of E_a for surface diffusion of Au under an applied potential fall in the range from 50 to 60 kJ/mol with decreasing trend with increasing potential [26] whereas it reaches 167 kJ/mol in a vacuum. The present intermediate values look appropriate for a free corrosion process although the varied E_a's obtained for de-alloying in concentrated HNO_3 solutions cannot be explained at the moment. The activation energy for the formation of ligaments using the amorphous alloy is 76 ± 17 kJ/mol [20], close to the above values for de-alloying of the crystalline alloy in consideration of the scatter in data for both cases. The D_s values are lower for the amorphous alloy apparently because of a varied pre-exponential factor which is dependent on the activation entropy [26], i. e. the difference in entropy between the activated state and the initial state of the atom. As discussed for the de-roughening process the pre-exponential factor vary widely according to the environment

where the crystal is with higher values in contact with the vacuum and lower when the moving atom interacts with an electrolyte. In the de-alloying of either crystalline or amorphous alloys the activated state should involve a relevant interaction with the electrolyte which will mostly determine the height of the activation barrier in both cases whereas the initial state differs: the case of Au atoms on the surface of an amorphous alloy implying more disorder. Care must be taken in handling these values in consideration of the scatter in data for both cases.

It is finally noted that in addition to de-roughening and coarsening of ligaments, the surface tension drives a further phenomenon: i. e. grain boundary grooving. Grooves form where the external surface meets grain boundaries by atomic movement away from the junction. The flux of atoms is described in an way analogous to de-roughening but in opposite direction [35]. Applying this concept to the present case of formation of ligaments by de-alloying an amorphous alloy, it is then expected that the flattening of the surface of ligaments ceases when local equilibrium at the triple junction is reached. The images in Fig. 2 may be representative of the different behaviour with respect to crystalline alloys due to the occurrence or absence of grain boundaries in the two cases although the process was conducted in the same conditions and to the same extent.

Conclusions

Two multicomponent Au-based alloys having respectively a crystalline and an amorphous structure have been de-alloyed by free corrosion in the same conditions leading to NPG. The morphology and size of ligaments and pores have been studied by XRD, Rietveld analysis and SEM images showing the coarsening of ligaments as a function of temperature and electrolyte concentration.

By comparing the ligament morphology between NPG from crystalline or amorphous precursor, differences in the de-alloying mechanism have been revealed: while for the crystalline alloy the etching retains the original grains on removing the less noble elements, in amorphous alloy the progressive removal of less noble elements liberates adatoms of Au that form aggregates with other noble atoms moving by surface diffusion. These domains grow as a function of the time until they impinge with other domains forming ligaments composed of several crystals. The morphology of ligaments is then dependent on the nature of the matrix from which it derives. In addition to the surface appearance of ligaments this is proven by the parameter *r*, defined as the ratio between the size of ligaments and scattering domains, which in the case of amorphous alloys is of the order of 5 while in the case of crystalline alloys is close to one. Furthermore, the surface diffusivity D_s and the activation energy for diffusion E_a have been discussed using a surface diffusion model of de-roughening Au electrodes: D_s result in the range found in literature, the activation energy is somewhat higher in comparison with de-alloying processes performed with an applied electrochemical potential, and the pre-exponential factor is lower for the amorphous alloy in relation to differences in entropy between the activated state and the initial state of the moving atom.

Acknowledgments

This work was supported by Convenzione Intesa SanPaolo-UNITO, NanoFacility Piemonte, and by the funding scheme of the European Commission, Marie Curie Actions — Initial Training Networks (ITN) in the frame of the project VitriMetTech — Vitrified Metals Technologies and Applications in Devices and Chemistry, 607080 FP7-PEOPLE-2013-ITN.

.

References

[1] Erlebacher J, Seshadri R. Hard Materials with Tunable Porosity. MRS Bulletin 2009;34(8):561-566.

[2] Lang XY, Guo H, et al. Novel Nanoporous Au-Pd Alloy with High Catalytic Activity and Excellent Electrochemical Stability. J.Phys. Chem. C 2010;114:2600–2603.

[3] Min H, Sullivan N, Allara D, Tadigadapa S. Nanoporous Gold: A High Sensitivity and Specificity Biosensing Substrate. Procedia Eng. 2011;25:1469–1472.

[4] Jin HJ, Weissmüller J, Bulk Nanoporous Metal for Actuation. Adv. Eng. Mater. 2010;12:714–723.

[5] Stratmann M, Rohwerder M. A pore view of corrosion. Nature 2001;410:420-423.

[6] Fritz JD, Pickering HW. Selective Anodic Dissolution of Cu-Au Alloys: TEM and Current Transient Study. J Electrochem. Soc. 1991;138:3209-3218.

[7] Erlebacher J, Aziz MJ, Karma A, Dimitov N, Sieradzki K. Evolution of nanoporosity in dealloying. Nature 2001;410:450-453.

[8] Lu X, Bischoff E, Spolenak R, Balk TJ. Investigation of dealloying in Au–Ag thin films by quantitative electron probe microanalysis. Scripta Materialia 2007;56:557-560.

[9] Erlebacher J, Sieradzki K. Pattern formation during dealloying. Scripta Materialia 2003;49:991-996.

[10] Erlebacher J. An Atomistic Description of Dealloying. J of the Electrochemical Society 2004;10:C614-C626.

[11] Pickering HW, Wagner C. Electrolytic Dissolution of Binary Alloys Containing a Noble Metal. J Electrochemical Science 1967;114:698-706.

[12] Pickering HW. Characteristic features of alloy polarization curves. Corrosion Science 1983;23:1107-1120.

[13] Sieradzki K. Curvature effects in Alloy Dissolution. J Electrochemical Society 1993; 140:2868-2872.

[14] Zhang Q, Wang X, Qi Z, Wang Y, Zhang Z. A benign route to fabricate nanoporous gold through electrochemical dealloying of Al–Au alloys in a neutral solution. Electrochim. Acta 2009;54:6190-6198.

[15] Yu J, Ding Y, Xu C, Inoue A, Sakurai T, Chen MW. Nanoporous Metals by Dealloying Multicomponent Metallic Glasses. Chem. Mater. 2008;20:4548–4550.

[16] Liu WB, Zhang SC, Li N, Zheng JW, Xing YL. Influence of phase constituent and proportion in initial Al–Cu alloys on formation of monolithic nanoporous copper through chemical dealloying in an alkaline solution. Corrosion Science 2011;53:809-814.

[17] Rizzi P, Scaglione F, Battezzati L. Nanoporous gold by dealloying of an amorphous precursor. J. Alloys and Comp. 2014;586S:S117–S120.

[18] Scaglione F, Rizzi P, Battezzati L. De-alloying kinetics of an Au-based amorphous alloys. J. Alloys and Comp. 2012;536S:S60–S64.

[19] Battezzati L, Moiraghi I, Calliari I, Dabalà M. Hardening phases in some Ni-free 14 carat white gold alloys. Intermetallics 2004;12:327-332.

[20] Scaglione F, Rizzi P, Celegato F, Battezzati L, Synthesis of nanoporous gold by free corrosion of an amorphous precursor. J. Alloys and Comp. 2014;615:S142–S147.

[21] Newman RC. Dealloying, Shreir's Corrosion, 4th Edition. Elsevier 2010;2:801-809.

[22] Lutterotti SML, Wenk HR. MAUD (Material Analysis Using Diffraction) is released under free license of the authors. <http://www.ing.unitn.it/wmaud/index.html>.

[23] Guo H, Zhang W, Qin C, et al. Glass-Forming Ability and Properties of New Au-Based Glassy Alloys with Low Au Concentrations. Materials Transactions 2009;50:1290-1293.

[24] Cheng YQ, Ma E. Atomic-level structure and structure–property relationship in metallic glasses. Progress in Materials Science 2011;56:379–473.

[25] Suryanarayana C, Inoue A. Bulk Metallic Glasses, CRC Press, Boca Raton, FL, 2011, Ch. 6.

[26] Vega AA, Newman RC. Nanoporous Metals Fabricated through Electrochemical Dealloying of Ag-Au-Pt with Systematic Variation of Au:Pt ratio. J. Electrochem. Soc. 2014;161:C1-C10.

[27] Present Authors, in preparation.

[28] Dona JM, Gonzalez-Velasco J. Mechanism of Surface Diffusion of Gold Adatoms in Contact with an Electrolytic Solution. J. Phys. Chem. 1993;97:4714-4719.

[29] Alonso C, Salvarezza RC, et al. The Surface Diffusion of Gold Atoms on Gold Electrodes in Acid Solution and its Dependence on the Presence of Foreign Adsorbates. Electrochem. Acta 1990;9:1331-1336.

[30] Zhang Z, Wang Y, et. al. Formation of ultrafine nanoporous gold related to surface diffusion of gold adatoms during dealloying of Al_2Au in an alkaline solution. Scripta Materialia 2010;62:137-140.

[31] Qian LH, Chen MW, Ultrafine nanoporous gold by low-temperature dealloying and kinetics of nanopore formation. Applied Physics Letters 2007;91:083105.
[32] Andreasen G, Nazzarro M, Ramirez J, Salvarezza RC, Arvia AJ. Kinetics of Particle Coarsening at Gold Electrode/Electrolyte Solution Interfaces Followed by In Situ Scanning Tunneling Microscopy. Journal of The Electrochemical Society 1996;143:466-471.
[33] Dursun A, Pugh DV, Corcoran SG. Dealloying of Ag-Au Alloys in Halide-Containing Electrolytes Affect on Critical Potential and Pore Size. J. Electrochem. Soc.2003;150:B355-B360.
[34] García MP, Gómez MM, et. al. Effect on the solution composition and the applied potential on the kinetics of roughness relaxation at gold electrodes in slightly acid electrolytes. J. Electroanal. Chem. 1993;347:237–246.
[35] Shewmon PG. Diffusion in Solids, Mc Grew-Hill, New York, 1963.

Table1 in supporting Information

Table 1

Conc. (M)	Temp. (K)	Ligament size (D)/(nm)	Scattering Domains (S_d)/(nm)	r D/S_d
5	255	22±6	25±1	0.69±0.21
	293	37±9	47±1	0.63±0.16
	343	116±28	115±2	1.00±0.26
	363	166±66	136±1	1.69±0.65
10	255	26±4	48±1	0.54±0.09
	293	41±11	60±1	0.48±0.14
	343	132±33	132±1	0.93±0.25
	363	168±43	156±3	1.21±0.35
14.4	255	46±12	45±1	1.03±0.30
	293	66±17	65±1	0.76±0.20
	343	139±32	107±1	1.39±0.33
	363	155±40	207±4	0.69±0.20

Table2 in supporting Information

Tab.2

Concentration [M]	Temp. (K)	Ligament size (D)/(nm)	Scat. Domains (S_d)/(nm)	r D/S_d
10	293	77±17	14±1	5.66±1.29
	313	81±17	17±1	4.82±1.04
	343	92±21	19±1	4.77±1.19
	363	142±43	38±1	3.78±1.16

Table3 in supporting Information

Table 3

Temperature K	Electrolyte concentration 14.4 M	10 M	5 M
255	$7.1 \cdot 10^{-21}$	$7.0 \cdot 10^{-22}$	$3.4 \cdot 10^{-22}$
293	$9.9 \cdot 10^{-19}$	$1.5 \cdot 10^{-19}$	$1.0 \cdot 10^{-19}$
343	$9.3 \cdot 10^{-17}$	$7.4 \cdot 10^{-17}$	$4.5 \cdot 10^{-17}$
363	$1.5 \cdot 10^{-16}$	$2.0 \cdot 10^{-16}$	$2.0 \cdot 10^{-16}$

Table4 in supporting Information

Table 4

Reference	Structure of the starting alloy	Sample	Electrolyte	E_a kJ mol^{-1}
[29] Z. Zhang	Crystalline	Al_2Au	20 wt.% NaOH	60.1±2.9
[27] J.M. Dona	Crystalline	Au	0.5 H_2SO_4	55.1-14.3
[28] C. Alonso	Crystalline	Au	0.5 H_2SO_4	59
[28] C. Alonso	Crystalline	Pt	0.5 H_2SO_4	79
[30] L.H. Qian	Crystalline	$Ag_{65}Au_{35}$	70% HNO_3	74±3
[20] F. Scaglione	Amorphous	$Au_{40}Cu_{28}Ag_7Pd_5Si_{20}$	10 M HNO_3	76±17

Figure(s)

Fig.1

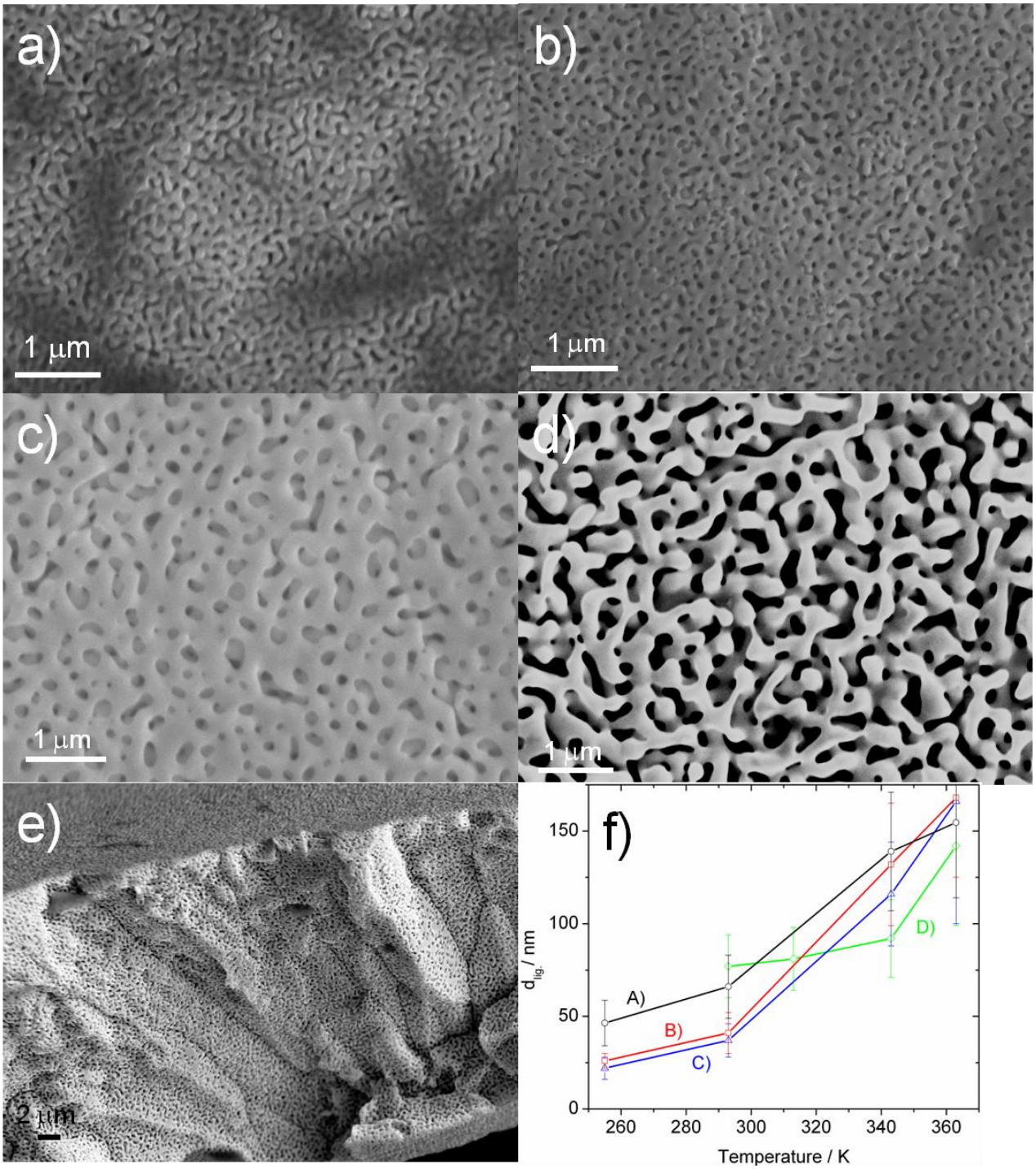

Fig. 2

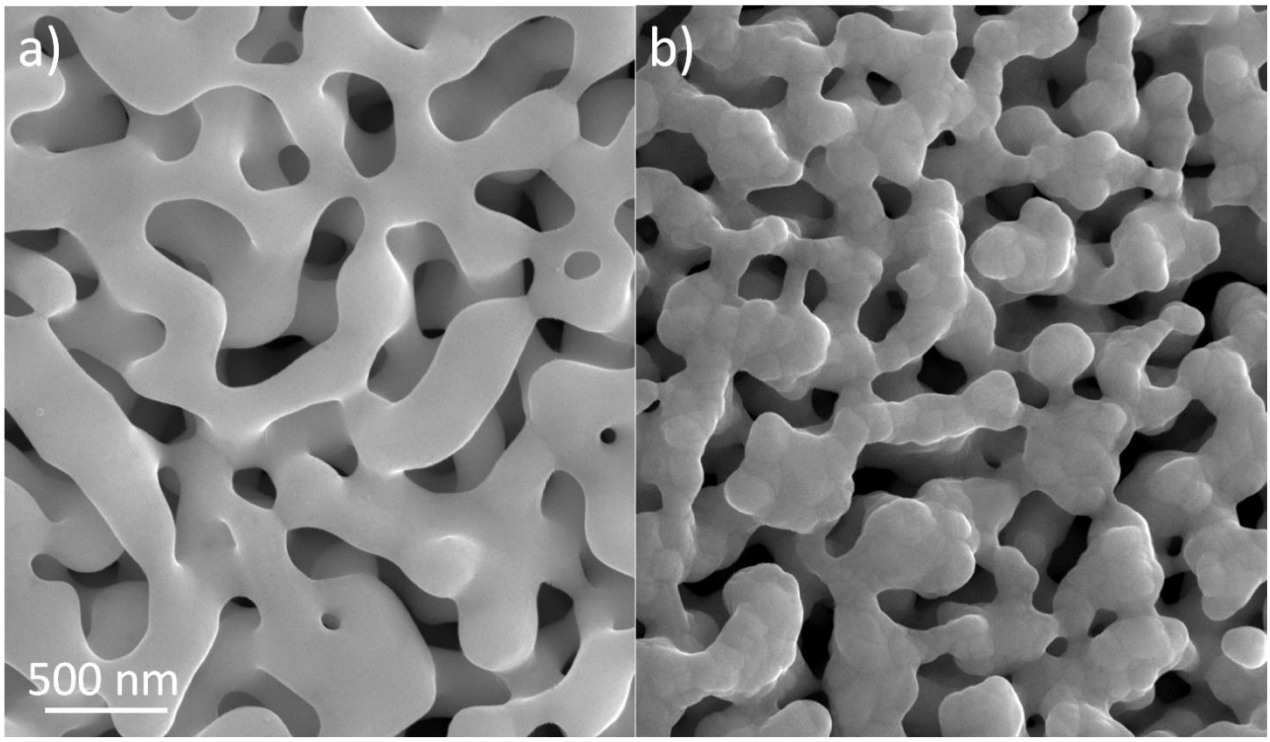

Fig.3

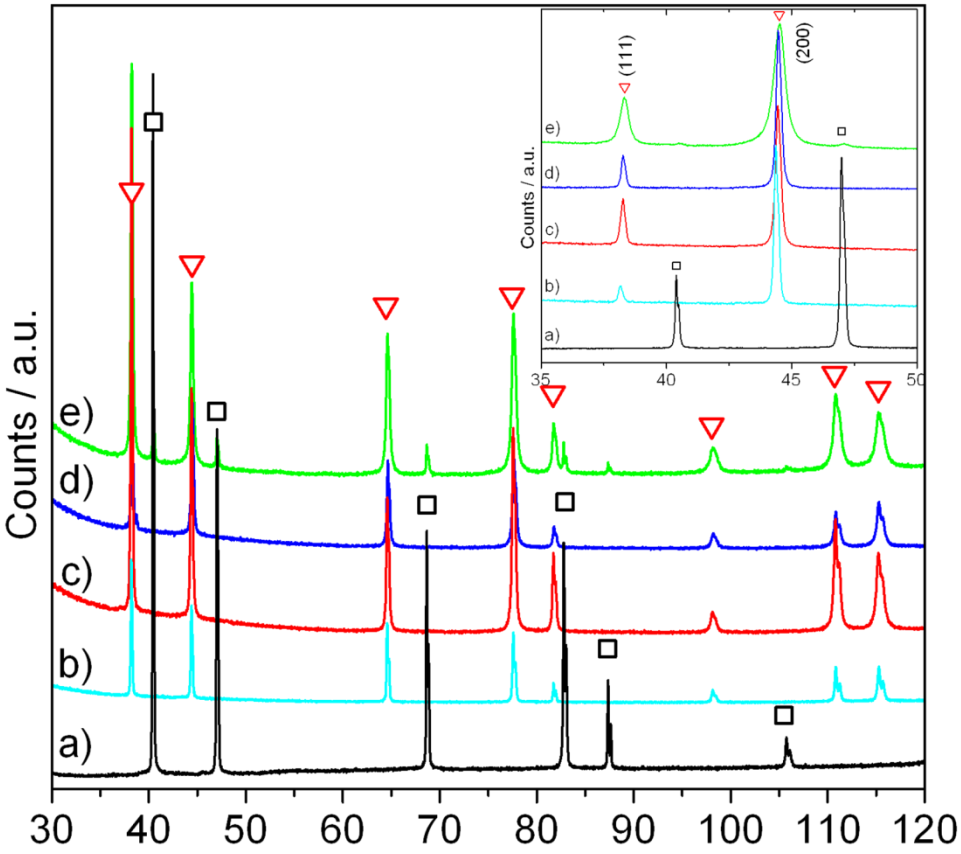
Counts / a.u.
e)
d)
c)
b)
a)
30
40
50
60
70
80
90
100
110
120
(111)
(200)
Counts / a.u.
35
40
45
50

Fig.4

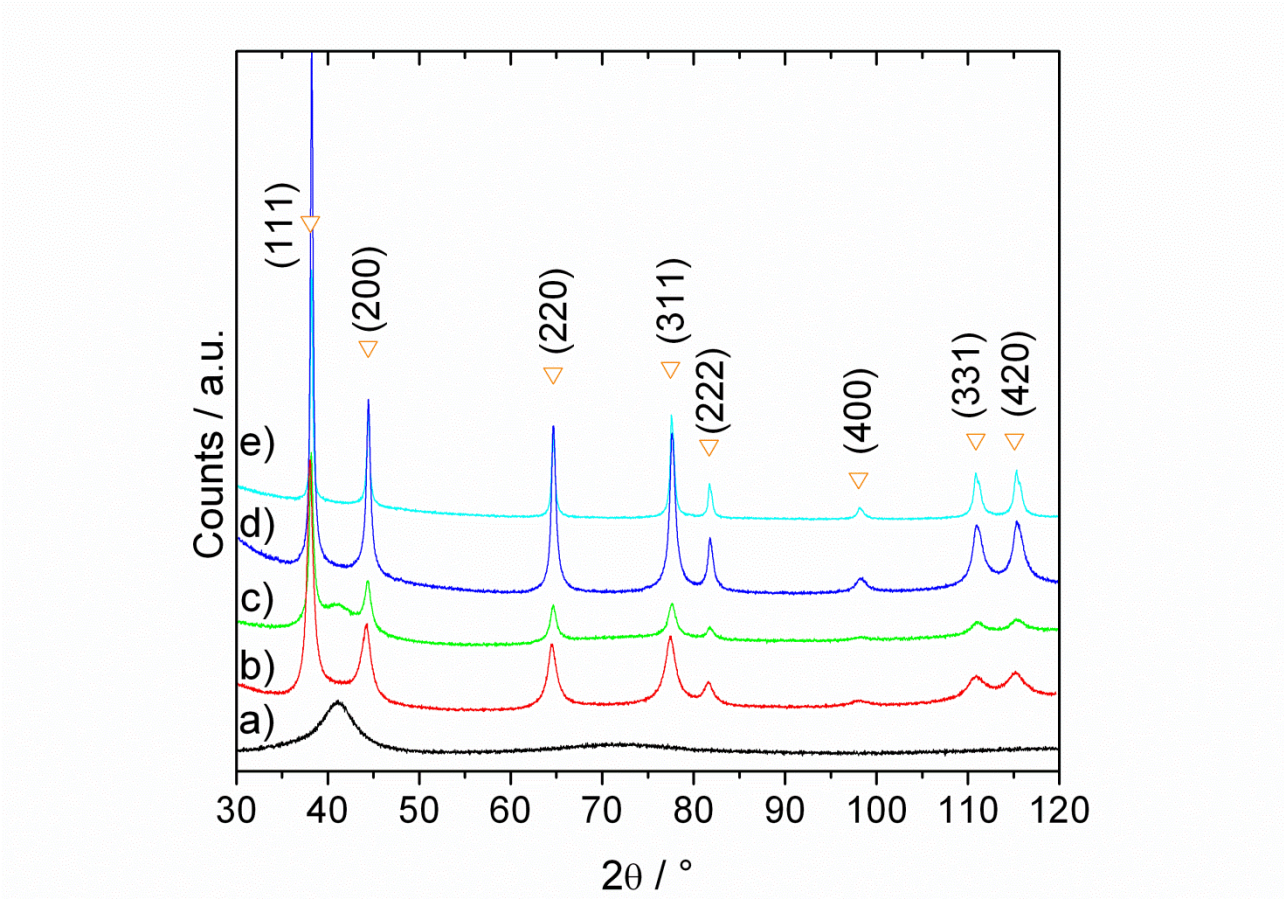
(111)
(200)
(220)
(311)
(222)
(400)
(331)
(420)
e)
d)
c)
b)
a)
Counts / a.u.
30
40
50
60
70
80
90
100
110
120
2θ / °

Fig.5

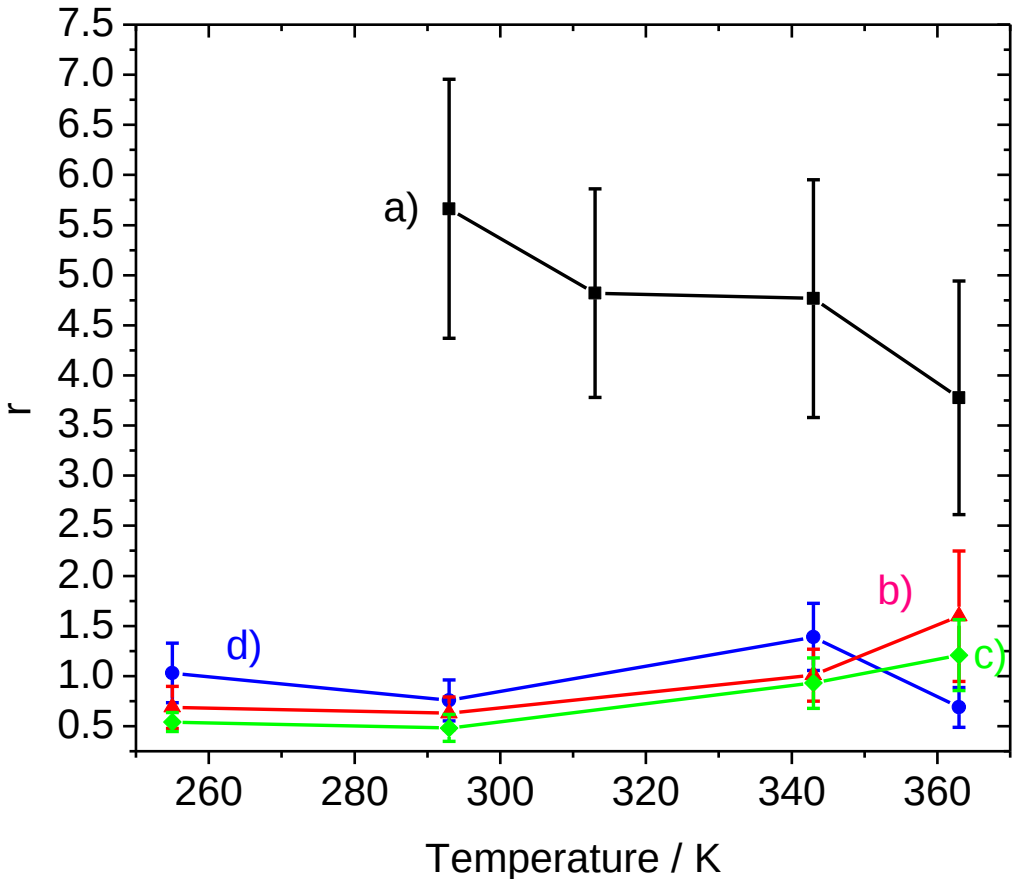
7.5
7.0
6.5
6.0
5.5
5.0
4.5
4.0
3.5
3.0
2.5
2.0
1.5
1.0
0.5
r
a)
b)
c)
d)
260
280
300
320
340
360
Temperature / K

Fig.6

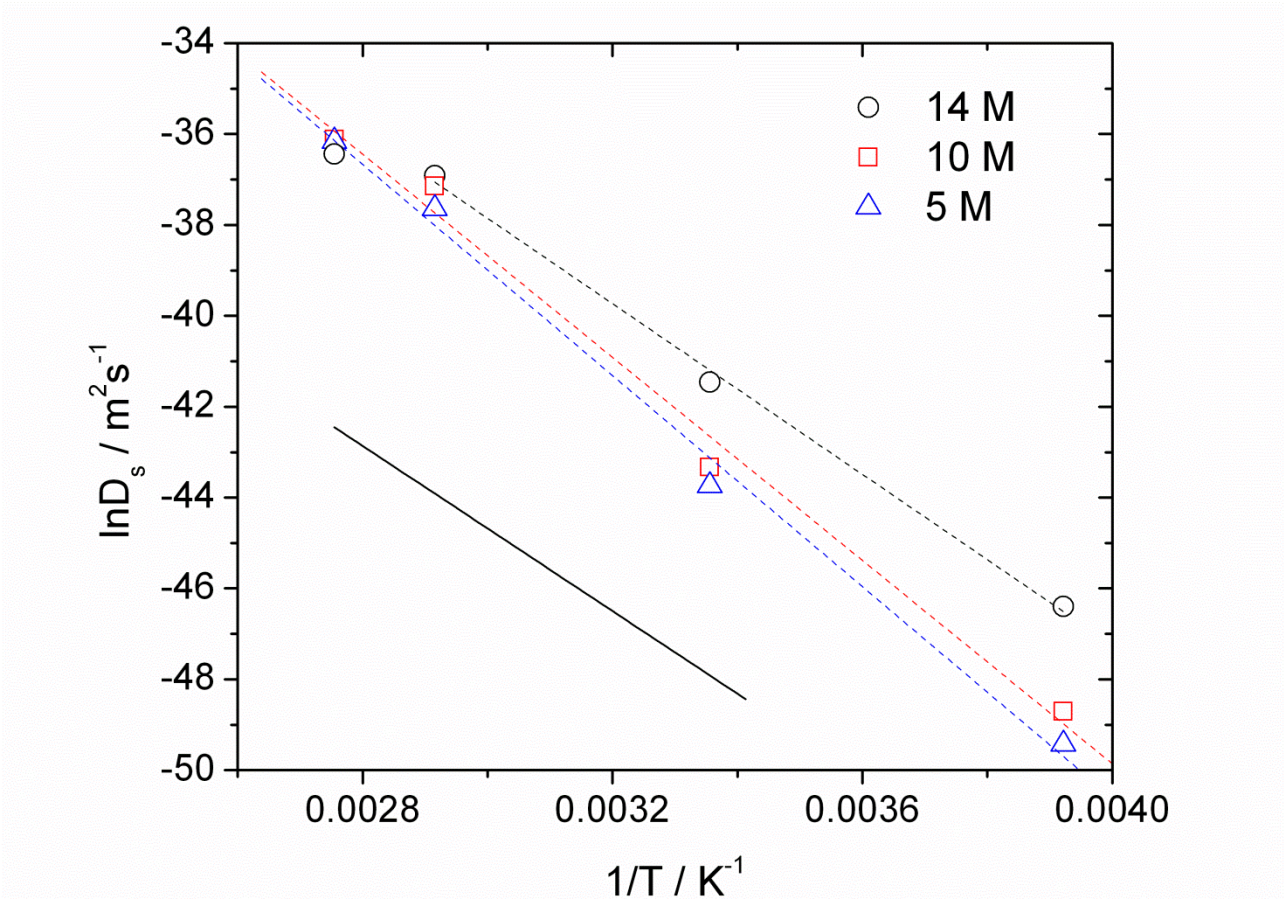
-34
-36
-38
-40
-42
-44
-46
-48
-50
lnD_s / m^2s^-1
0.0028
0.0032
0.0036
0.0040
1/T / K^-1
14 M
10 M
5 M

Highlights

1) NPG made by free corrosion of a crystalline and an amorphous Au-based alloys

2) Coarsening of ligaments as a function of temperature and electrolyte concentration

3) Difference in de-alloying mechanism in crystalline or amorphous precursor outlined

4) Ligaments morphology changes with the matrix from which they derive

5) Kinetics of de-alloying determined

Figures Caption

Images captions

Fig.1. Top view of the $Au_{31}Cu_{41}Zn_{12.8}Mn_{15.2}$ crystalline alloy after free corrosion in 14.4 M HNO_3 at a) 255 K, b) 293 K, c) 343 K, d) 363 K, e) 363 K, cross section. In f) the average size of ligaments is reported as a function of temperature in A) 14.4 M, B) 10 M, C) 5 M HNO_3. Data marked D) are for de-alloying in 10 M HNO_3 the $Au_{40}Cu_{28}Ag_7Pd_5Si_{20}$ amorphous alloy.

Fig.2. Close-up image of ligaments and pores obtained from de-alloying of a) the $Au_{31}Cu_{41}Zn_{12.8}Mn_{15.2}$ crystalline and b) the $Au_{40}Cu_{28}Ag_7Pd_5Si_{20}$ amorphous alloy.

Fig.3. XRD patterns taken on the wheel side of the as-spun $Au_{31}Cu_{41}Zn_{12.8}Mn_{15.2}$ ribbon a) and on samples de-alloyed in 14.4 M HNO_3 at 363 b), 343 c), RT d) and 255 K e). A detail of patterns showing the texture on the air side is given in the inset. Symbols: □ as-spun and ∇ de-alloyed.

Fig.4. XRD pattern of the $Au_{40}Cu_{28}Ag_7Pd_5Si_{20}$ amorphous alloy a) as spun and after de-alloying in 10 M HNO_3 at b) 293 K, c) 313 K, d), 343 K c) and d) and 363 K.

Fig.5 The ratio of the size of scattering domains to that of ligaments vs T for a) $Au_{40}Cu_{28}Ag_7Pd_5Si_{20}$ free corroded in 10 M HNO_3 and $Au_{31}Cu_{41}Zn_{12.8}Mn_{15.2}$ free corroded in b) 5 M, c) 10 M and d) 14.4 M HNO_3.

Fig.6. Arrhenius plot of ln Ds vs. T^{-1}. Dashed lines are fits to the data for the de-alloyed $Au_{31}Cu_{41}Zn_{12.8}Mn_{15.2}$ crystalline alloy in 5, 10 and 14.4 M HNO_3; full line is from fitting the data for the de-alloyed $Au_{40}Cu_{28}Ag_7Pd_5Si_{20}$ amorphous precursor in 10 M HNO_3 [20].

Figures and Tables Caption of supporting information

Supporting information captions

Fig.S1 SEM images of pores and ligaments after free corrosion of $Au_{31}Cu_{41}Zn_{12.8}Mn_{15.2}$ in 10 M HNO_3 at 255, 293, 343 and 363 K, surface-view and cross section details.

Fig.S2 SEM images of pores and ligaments after free corrosion of $Au_{31}Cu_{41}Zn_{12.8}Mn_{15.2}$ in 5 M HNO_3 at 255, 293, 343 and 363 K, surface-view and cross section details.

Fig.S3. XRD patterns taken on the wheel side of the as-spun $Au_{31}Cu_{41}Zn_{12.8}Mn_{15.2}$ ribbon a) and on samples de-alloyed in 10 M HNO_3 at 363 b), 343 c), RT d) and 255 K e). A detail of patterns showing the texture on the air side is given in the inset. Symbols: □ as-spun and ∇ de-alloyed.

Fig.S4. XRD patterns taken on the wheel side of the as-spun $Au_{31}Cu_{41}Zn_{12.8}Mn_{15.2}$ ribbon a) and on samples de-alloyed in 5 M HNO_3 at 363 b), 343 c), RT d) and 255 K e). A detail of patterns showing the texture on the air side is given in the inset. Symbols: □ as-spun and ∇ de-alloyed.

Fig.S5. HRTEM image of a sample of amorphous $Au_{40}Cu_{28}Ag_7Pd_5Si_{20}$ de-alloyed for 30 s in 1 M HNO_3. Lattice fringes due to random fine crystals of nanometer size are widespread in the viewing area.

Fig.S6. HRTEM image of a sample of amorphous $Au_{40}Cu_{28}Ag_7Pd_5Si_{20}$ de-alloyed for 5 min in 1 M HNO_3. Lattice fringes due to random crystals are seen. Coalescence of crystals into ligaments and pores starts becoming apparent.

Table 1. Ligament size, scattering domains and their ratio *r* for the $Au_{31}Cu_{41}Zn_{12.8}Mn_{15.2}$ crystalline alloy after de-alloying treatment. Ligaments have been evaluated from high resolution SEM images while scattering domains from Rietveld analyses of the relative XRD patterns.

Table 2. Ligament size, scattering domains and their ratio *r* for $Au_{40}Cu_{28}Ag_7Pd_5Si_{20}$ the amorphous alloy after de-alloying treatments. Ligaments have been evaluated from hi resolution SEM images while scattering domains from Rietveld analyses of the relative XRD patterns. Data reported from literature [20].

Table.3 Surface diffusion coefficients obtained for the de-alloyed $Au_{31}Cu_{41}Zn_{12.8}Mn_{15.2}$ crystalline alloy at different condition of free corrosion de-alloying. Coefficients are expressed in m^2s^{-1}.

Table.4 Values of E_a obtained for crystalline and amorphous Au-based alloys from the literature.